ChemPubSoc Europe

DOI: 10.1002/cctc.201901640

CHEMCATCHEM Full Papers

Investigating the Active Species in a [(R-SN(H)S-R)$CrCl_3$] Ethene Trimerization System: Mononuclear or Dinuclear?

Bas Venderbosch,[a] Jean-Pierre H. Oudsen,[a] David J. Martin,[a] Bas de Bruin,[b] Ties J. Korstanje,[a] and Moniek Tromp*[a, c]

Cr-catalyzed ethene trimerization is an industrially important process to produce 1-hexene. Despite its industrial relevance, the changing oxidation state and the structural rearrangements of the metal center during the catalytic cycle remain unclear. In this study, we have investigated the active species in a [(R-SN(H)S–R)$CrCl_3$] (R = $C_{10}H_{21}$) catalyzed ethene trimerization system using a combination of spectroscopic techniques (XAS, EPR and UV/VIS) and DFT calculations. Reaction of the octahedral Cr^{III} complex with modified methylaluminoxane (MMAO) in absence of ethene gives rise to the formation of a square-planar Cr^{II} complex. In the presence of ethene (1 bar), no coordination was observed, which we attribute to the endergonic nature of the coordination of the first ethene molecule. Employing an alkyne as a model for ethene coordination leads to the formation of a dinuclear cationic Cr^{III} alkyne complex. DFT calculations show that a structurally related dinuclear cationic Cr^{III} ethene complex could form under catalytic conditions. Comparing a mechanism proceeding via mononuclear cationic Cr^{II}/Cr^{IV} intermediates to that proceeding via dinuclear cationic Cr^{II}/Cr^{III} intermediates demonstrates that only the mechanism involving mononuclear cationic Cr^{II}/Cr^{IV} intermediates can correctly explain the observed product selectivity.

1. Introduction

Several large chemical companies are faced with an increase in demand for the shorter (1-butene, 1-hexene and 1-octene) linear alpha olefins (LAOs) due to their application as a comonomer in the production of linear low-density polyethylene (LLDPE).[1,2] Traditionally, LAOs are produced by ethene oligomerization catalysts which generate a statistical product distribution, e.g. the nickel-based SHOP catalyst.[3] However, due to the growing market demand for shorter LAOs, several companies (e.g. Sasol and Chevron Phillips Chemical) have successfully commercialized chromium catalysts that are capable of selectively forming 1-hexene.[4,5]

An early mechanistic proposal has suggested the involvement of metalacyclic intermediates to explain the observed product selectivity (Scheme 1) and this proposal has been validated via deuterium labeling experiments.[6,7] However, the oxidation state of chromium during the catalytic cycle is still subject to debate. In the literature, some studies suggest a Cr^{I}/Cr^{III} redox couple and other studies suggest a Cr^{II}/Cr^{IV} redox couple to be responsible for the observed product selectivity.[8–13] None of these studies are however conclusive as no intermediates in the catalytic cycle have been directly detected. Various electron paramagnetic resonance (EPR) spectroscopy experiments have been performed in the presence of

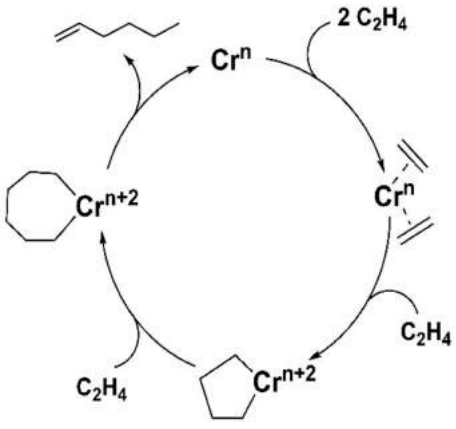

Scheme 1. Proposed mechanism for the selective trimerization of ethene to form 1-hexene. The mechanism is believed to proceed either via a Cr^{I}/Cr^{III} or Cr^{II}/Cr^{IV} redox couple.

[a] B. Venderbosch, J.-P. H. Oudsen, Dr. D. J. Martin, Dr. T. J. Korstanje, Prof. M. Tromp
Sustainable Materials Characterization
Van 't Hoff Institute for Molecular Sciences
University of Amsterdam
Science Park 904
Amsterdam 1098XH (The Netherlands)
[b] Prof. B. de Bruin
Homogeneous, Supramolecular and Bio-Inspired Catalysis
Van 't Hoff Institute for Molecular Sciences
University of Amsterdam
Science Park 904
Amsterdam 1098XH (The Netherlands)
[c] Prof. M. Tromp
Materials Chemistry
Zernike Institute for Advanced Materials
University of Groningen
Nijenborgh 4
Groningen 9747AG (The Netherlands)
E-mail: moniek.tromp@rug.nl

Supporting information for this article is available on the WWW under https://doi.org/10.1002/cctc.201901640

This publication is part of a Special Collection on "Advanced Microscopy and Spectroscopy for Catalysis". Please check the ChemCatChem homepage for more articles in the collection.

ethene in an attempt to observe some of these intermediates.[7,11,12,14] In none of these studies, novel resonances were observed that could be assigned to intermediates in the catalytic cycle. Possibly, these studies were hampered by (X-band) EPR-silence of (some of) the intermediates formed (e.g. dinuclear Cr^{I} or mononuclear Cr^{II} complexes).[15]

A technique that does allow for the detection of complexes that are unobservable by low-field EPR spectroscopy is X-ray Absorption Spectroscopy (XAS). XAS is a bulk technique that is sensitive to both the oxidation state and the coordination environment of the metal center.[16,17] This technique was applied by Brückner and coworkers in the study of the activation of a {Cr(PNP)} system and the formation of a neutral $[(PNP)Cr^{II}(Me)_2]$ complex was suggested.[12]

Recently, we have developed a freeze-quench XAS technique which allows for the trapping of reactive complexes.[18–20] Freeze-quench XAS is required to study these ethene trimerization systems due to catalyst deactivation occurring on the same timescale as a high-quality EXAFS data acquisition times (several hours). The freeze-quench methodology allows for 'trapping' of reaction intermediates at different points in time, i.e. obtaining time-resolution, while freezing these intermediates allows long measurement times required for high quality data. We have previously applied this technique to study the reaction of a {Cr(SNS)} ethene trimerization system with excess $AlMe_3$ and demonstrated that the octahedral Cr^{III} precursor is reduced to a Cr^{II} square-planar complex (Scheme 2).[21] This study was performed in the absence of ethene. The presence of ethene could promote further reactivity to the metal center.

The aim of the present study is to gain more insight into the oxidation state and the structure of the active species in the $[(R\text{-}SN(H)S\text{–}R)CrCl_3]$ ($R = C_{10}H_{21}$) ethene trimerization system. This was investigated by studying the activation of the Cr^{III} precursor using a variety of activators (e.g. $AlMe_3$ and MMAO-12) in the absence and presence of a suitable substrate (ethene, other alkenes and alkynes). Spectroscopic techniques that were employed to investigate the oxidation state and structure of the formed intermediates include X-band EPR, Cr K-edge XAS and UV/VIS. The spectroscopic data was interpreted by performing DFT–D3 calculations. The obtained results suggest that a dinuclear complex could form under catalytic conditions. Therefore, we performed DFT–D3 calculations to compare a mechanism proceeding via mononuclear intermediates to a mechanism proceeding via dinuclear intermediates.

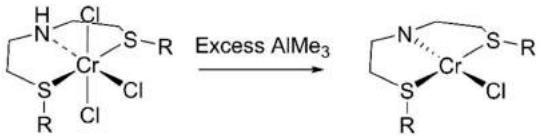

Scheme 2. Activation of $[(R\text{-}SN(H)S\text{–}R)CrCl_3]$ ($R = C_{10}H_{21}$) in the presence of excess $AlMe_3$ to yield a square-planar Cr^{II} intermediate, as reproduced from reference 21.

Table 1. Overview of the performance of **1** in the presence of various activators under one atmosphere of ethene in toluene.[a]

Entry	Activator	T [°C]	1-C_6 [mg][b]	TOF [h^{-1}][c]	PE [mg]
1	$AlMe_3$ (20 eq.)	RT	None	None	None
2	$AlMe_3$ (20 eq.)	50	None	None	None
3	$AlMe_3$ (20 eq.) Ph_3C^+ (1.2 eq.)	RT	0.07	0.2	0.2
4[d,e]	$AlMe_3$ (20 eq.) Ph_3C^+ (1.2 eq.)	50	9	20	None
5[e]	MMAO (400 eq.)	RT	12	29	10
6[e]	MMAO (400 eq.)	50	113	270	64
7[e,f]	$AlMe_3$ (40 eq.) MMAO (400 eq.)	50	230	546	0.32

[a] Reaction volume: 12 mL in toluene, reaction time: 60 minutes, internal standard: mesitylene (~3 mg/mL), catalyst amount: 5 µmol. Ph_3C^+ is used to denote $[Ph_3C][Al\{OC(CF_3)_3\}_4]$, [b] 1-$C_6$ is used to denote 1-hexene, [c] TOF is defined as the formation of mmol 1-hexene per mmol Cr per hour, [d] The catalyst was activated by addition of $AlMe_3$, after which the Ph_3C^+ source was quickly added (< 10 s), [e] Small quantities of decenes were observed in the GC, but these were not quantified, [f] The catalyst was activated by addition of $AlMe_3$. After 5 minutes of reaction time, the required amount of MMAO was injected.

2. Results and Discussion

2.1. Effect of the Activator on Catalytic Performance

To assess the performance of the catalytic system, we performed catalytic experiments under one bar of ethene pressure in toluene (Scheme 3 and Table 1). The catalyst was an *n*-decyl substituted $[(R\text{-}SN(H)S\text{–}R)CrCl_3]$ **(1)** complex.[22] As an activator we employed $AlMe_3$, $AlMe_3$ and $[Ph_3C][Al\{OC(CF_3)_3\}_4]$, and MMAO-12 (from now on denoted as MMAO) as activator.[23,24] MMAO was used as an industrially preferred activator. $AlMe_3$, and $AlMe_3$ and $[Ph_3C][Al\{OC(CF_3)_3\}_4]$ were used as more well-defined activators.[25]

The choice of activator has a large influence on the performance of the catalyst. When **1** is activated with $AlMe_3$

Scheme 3. An overview of the catalyst (**1**) and activators (**a**–**c**) employed in this study. For the catalyst, $[(R\text{-}SN(H)S\text{–}R)CrCl_3]$ ($R = C_{10}H_{21}$) was used. For the activators, $AlMe_3$ (**a**), $AlMe_3$ and $[Ph_3C][Al\{OC(CF_3)_3\}_4]$ (**b**) and MMAO (**c**) were employed.

(20 eq.) no activity is observed at room temperature or 50 °C (entry 1 and 2). If **1** is first reacted with $AlMe_3$ (20 eq.) and quickly afterwards (< 10 s) reacted with the Lewis acid, $[Ph_3C][Al\{OC(CF_3)_3\}_4]$ (1.2 eq.), the catalyst does become active at an elevated temperature of 50 °C (entry 3 and 4). When MMAO (400 eq.) is employed as an activator for **1**, a significant increase in productivity of the catalyst is observed. The MMAO-activated catalyst is already active at room temperature (entry 5). Increasing the reaction temperature to 50 °C further increases the activity (entry 6). In addition to formation of 1-hexene, formation of a relatively large quantity of polyethylene (PE) is observed.

In Ti^{IV} ethene trimerization systems it is known that partially alkylated Ti^{IV} species are responsible for polymer formation. In these Ti systems, the amount of PE produced can be reduced by pre-alkylation of the metal center.[26] In this {Cr(SNS)} system, we can significantly decrease the amount of PE (entry 7) formed by first pre-activating **1** with $AlMe_3$ (20 eq.) and subsequently introducing MMAO (400 eq.) into the reaction mixture. In that case a minimal amount of PE is observed while retaining high activity. In a patent publication it was also demonstrated that activation of a $[(R\text{-}SN(H)S\text{–}R)CrCl_3]$ complex with a mixture of $AlMe_3$ and MAO can lead to reduced PE formation.[5,27]

The obtained catalytic results show that the presence of Lewis acidic sites within the reaction mixture is important to generate an active catalyst. When no additional Lewis acidic sites are introduced (entry 1 and 2), no active catalyst is obtained. When Ph_3C^+ cations or MMAO is introduced into the reaction mixture (entry 3–7), an active catalyst is obtained. McGuinness *et al.* also investigated the effect of Lewis acids on the catalytic performance of the {Cr(SNS)} ethene trimerization system. They also observed a positive effect of Lewis acids on catalytic performance. In addition, they found $\{Cr^{II}(SNS)\}$ complexes to be active for selective ethene trimerization. Based on these results the authors have suggested a cationic Cr^{II}/Cr^{IV} redox couple to be operative in the {Cr(SNS)} system.[23]

2.2. Spectroscopic Investigation of the Activation Process in the Absence of a Substrate

The activation of **1** using $AlMe_3$, $AlMe_3$ and $[Ph_3C][Al\{OC(CF_3)_3\}_4]$ and MMAO was studied in toluene in the absence of ethene using a variety of spectroscopic techniques (X-band EPR, stopped-flow UV/VIS and Cr K-edge XAS). We had already investigated the activation of **1** with $AlMe_3$ and $AlMe_3$ and $[Ph_3C][Al\{OC(CF_3)_3\}_4]$ in a previous study and observed the formation of a square-planar Cr^{II} complex with a deprotonated amine functionality (Scheme 2).[21] In this study, we have reproduced these experiments. The results are reported in the Supporting Information (Section 2.2 and Section 2.3) and the obtained results are in line with our previous study.

In this study, we have also investigated the activation of **1** with MMAO (400 eq.). The results are reported in detail in the Supporting Information (Section 2.4). Bond distances for solutions of **1** and **1** activated with MMAO in toluene (frozen after 2 minutes) obtained via Cr K-edge EXAFS analysis are compared in Table 2. Similar coordination numbers and bond distances are observed when **1** is activated with either MMAO (Table 2), $AlMe_3$, or $AlMe_3$ and $[Ph_3C][Al\{OC(CF_3)_3\}_4]$ (Supporting Information Section 2.2 and 2.3). These results indicate that a square-planar Cr^{II} complex is also formed when **1** is activated with MMAO (Scheme 2). In addition to the formation of a square-planar Cr^{II} complex, the formation of a bis(η^6-tolyl)Cr^{I} complex is detected with X-band EPR spectroscopy (Figure S19 and Figure S20a). The concentration of the bis(η^6-tolyl)Cr^{I} complexes increases with time. After roughly an hour, the concentration is close to 10% of the total chromium content (Figure S20b). The formation of these bis(η^6-tolyl)Cr^{I} complexes is a known deactivation pathway in the selective trimerization of ethene.[14,20]

Using DFT–D3 calculations at the BP86/TZP level of theory we have studied the thermochemistry of the reduction of **1** via reaction with trialkylaluminum compounds (Supporting Information 3). Reduction was assumed to proceed via reaction of the complex with free $AlMe_3$ contained within MMAO, as $AlMe_3$ has a higher alkylation aptitude.[28,29] Our results are summarized in Scheme 4 and Table 2. Shown is the thermodynamically most favored structure taking account retention (model A) and deprotonation (model B) of the amine functionality. The calculated Cr–N distance of model B is in close agreement with the experimentally observed Cr–N distance, making it likely that the amine is deprotonated.

We also considered the interaction of Lewis acids ($AlMe_3$, Ph_3C^+ and MMAO) with lone pairs contained on the chloride and amide moiety (Scheme 4, model C–G). For MMAO we used a model with the general structure $(AlOMe)_{10}.AlMe_3$ recently

Table 2. Overview of structural parameters obtained from DFT–D3 calculations at the BP86/TZP level of theory level for various Cr^{II} complexes (Scheme 4) in the gas phase compared to the experimentally obtained Cr K-edge EXAFS data.[a]

Model	Coordination shell	*d* (Cr–X) [Å]
Experimental EXAFS data (**1**) [b]	1 Cr–N	2.15(4)
	5 Cr–Cl/Cr–S	2.35(1)
Experimental EXAFS data	1.2(4) Cr–N	2.06(2)
(**1** + MMAO (400 eq.); 2 min.) [a]	3 Cr–Cl/Cr–S	2.43(1)
1	1 Cr–N	2.186
	5 Cr–Cl/Cr–S	2.393
A	1 Cr–N	2.211
	4 Cr–Cl/Cr–S	2.443
B	1 Cr–N	2.003
	3 Cr–Cl/Cr–S	2.404
C	1 Cr–N	1.984
	3 Cr–Cl/Cr–S	2.435
D	1 Cl–N	2.116
	3 Cr–Cl/Cr–S	2.393
E	1 Cr–N	2.097
	3 Cr–Cl/Cr–S	2.422
F	1 Cr–N	1.943
	3 Cr–Cl/Cr–S	2.394
G	1 Cr–N	1.977
	3 Cr–Cl/Cr–S	2.446

[a] For the calculated Cr–Cl/Cr–S distance, an average of the Cr–S and Cr–Cl distance is reported. [b] Given is the experimental (Cr-X) (Å) distance, as is obtained from Cr K-edge EXAFS measurements. Samples were measured as frozen toluene solutions (100 K). Full analysis details can be found in the ESI.

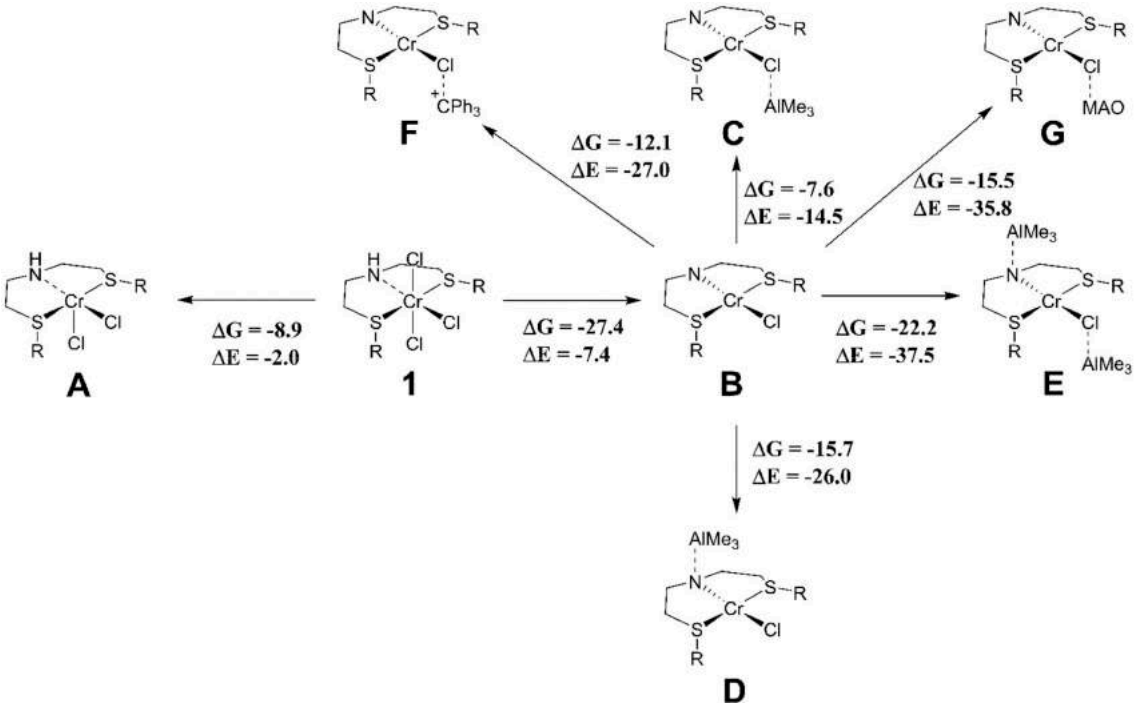

Scheme 4. Calculated structures that were used to compare to the experimental bond distances. Gibbs free energies (ΔG) and electronic energies (ΔE) are reported in kcal mol^{-1} for the high-spin states of the depicted complexes. Frequency calculations were performed at 298.15 KDFT-D3 calculations were performed at the BP86/TZP level of theory in the gas phase. Full calculations are found in the Supporting Information (Section 3). Selected structural parameters are.

described by Zurek and coworkers.[30] For all considered geometries, interaction of the complex with the Lewis acids was found to be highly exergonic. However, due to the close similarity of the calculated bond distances for the various models, we cannot conclusively assign a single model to our experimental XAS data (*vide supra*).

2.3. Spectroscopic Investigation of the Activation Process in the Presence of a Substrate

With an understanding of the structure of the metal complex after activation, we set out to study the reactivity of the metal complex towards C_2H_4 using Cr K-edge XAS spectroscopy. Cr K-edge XAS experiments were done via activation of the metal center in the presence of C_2H_4 (1 bar) and freezing these solutions after a set reaction time. The results are depicted in Figure 1.

Initially, activation experiments were performed at room temperature in the presence of C_2H_4 (1 bar) using $AlMe_3$ (40 eq.) and $[Ph_3C][Al\{OC(CF_3)_3\}_4]$ (1.2 eq.), and MMAO (400 eq.) as activator. Under these conditions no changes are observed in the XANES (Figure 1a and c) and EXAFS region (Figure 1b and d). Therefore, we performed experiments at −50 °C and 50 °C. A temperature of −50 °C was chosen to overcome a (potentially) entropically disfavored coordination of ethene to the metal center. A temperature of 50 °C was chosen, as the catalyst is more active at this temperature (Table 1). In most experiments, no differences are observed between the individual spectra. The XANES region for **1** activated with MMAO (400 eq.) at 50 °C does show minor differences. The XANES region matches closely with the XANES region of samples aged for 3 h and 12 h in the absence of ethene (Figure S41). Based on quantitative EPR measurements, relatively large quantities of bis(η^6-tolyl)Cr^{I} are expected after 3 h (~7%) and 12 h (~18%). We therefore attribute these differences in the Cr K-edge XANES region to an increase in concentration of bis(η^6-tolyl)Cr^{I} at elevated temperatures.

These observations lead to two hypotheses: i) either the first ethene coordination event is endergonic in nature and coordination of ethene cannot be observed in the experiment as performed or ii) a minority species is responsible for catalysis and the majority species is incapable of coordinating ethene. The first hypothesis is in line with a recent kinetic study of a {Cr(PN)} ethene tetramerization system, where it is demonstrated that the first and/or the second ethene coordination event is reversible.[31] The second hypothesis has been proposed by Bercaw and coworkers in a {Cr(PNP)} ethene trimerization system.[32]

To investigate the first hypothesis, we resorted to different substrates. As discussed earlier, catalytic tests hint at a cationic mechanism being operative in this ethene trimerization system due to the observed positive effect of Lewis acids. Three free coordination sites are required on the metal center to successfully complete the catalytic cycle for a tridentate ligand (Scheme 1). We therefore envisioned an initiation pathway,

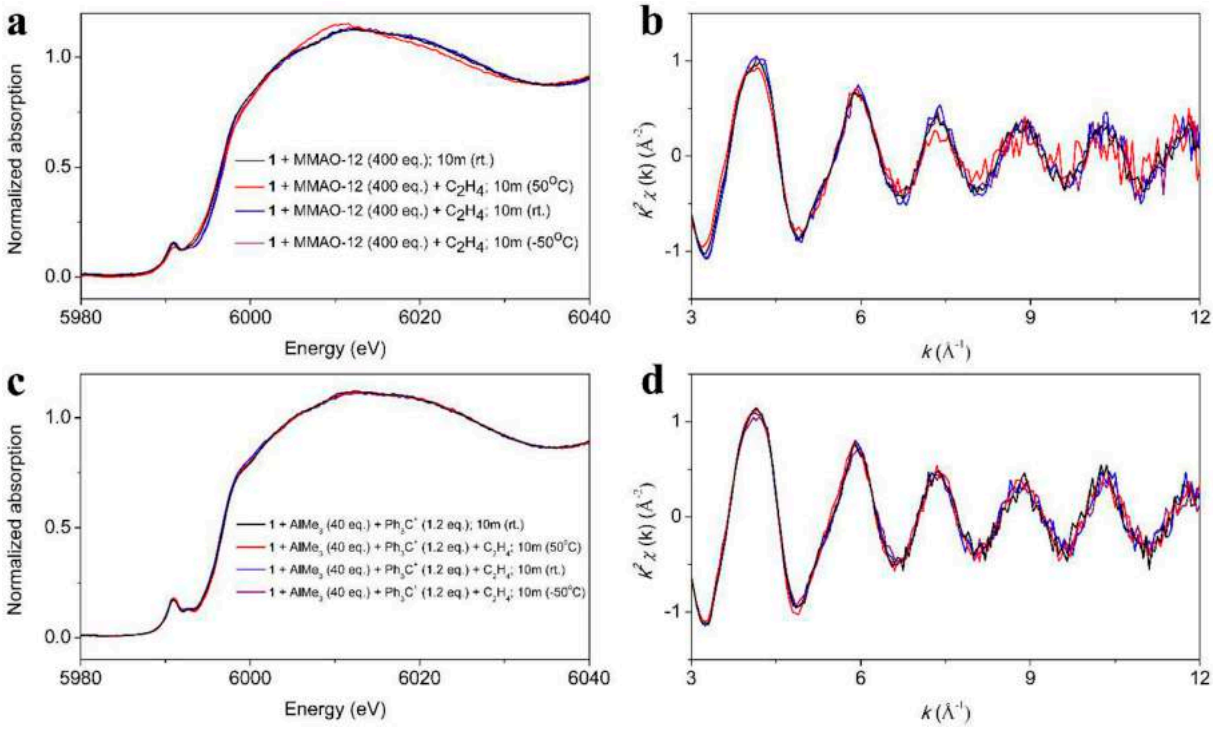

Figure 1. Cr K-edge XAS experiments performed in the presence of ethene (1 bar) with various activators. a) XANES and b) EXAFS region of activation experiments with MMAO (400 eq.) in the presence and absence of ethene at various temperatures. c) XANES and b) EXAFS region of activation experiments with $AlMe_3$ (40 eq.) and $[Ph_3C][Al\{OC(CF_3)_3\}_4]$ (1.2 eq.) in the presence and absence of ethene at various temperatures. The samples were measured as a frozen solution in toluene in fluorescence mode. The legend is only shown in Figure 1a and 1c. A similar coloring scheme is used in Figure 1b and d.

where the halide is abstracted from the metal center and a cationic, electron-poor metal center is generated (Scheme 5). To this cationic metal center, ethene can subsequently coordinate. Generation of a cationic metal center in solvents with low dielectric constants (e.g. toluene) is expected to be disfavored.[33] To stabilize such a cationic complex, we turned our attention to more electron-rich substrates.

Initial tests were done with 1-octene and 2,3-dimethyl-2-butene. Upon addition of these olefins to a MMAO-activated solution (400 eq.) of **1**, no changes in the UV/VIS spectra were observed after 2 h (Figure S42). In a previous study, Bercaw and coworkers have demonstrated that ethene trimerization systems can also be employed as alkyne cyclotrimerization catalysts.[7] Upon activation of **1** with MMAO (400 eq.) or with $AlMe_3$ (40 eq.) and introducing 3-hexyne (60 eq.), an immediate color change from green to orange is observed. Heating the solution to 70 °C and letting the mixture react for 1 h allows for the formation of hexaethylbenzene, as is observed by ^{1}H NMR spectroscopy (Figure S40). The proposed mechanism of chromium-catalyzed cyclotrimerization (Scheme 6) shows similarities to the trimerization of ethene and alkynes might therefore be used as a model for the reactivity of ethene.[34,35] For our spectroscopic investigation, we employed 1-phenyl-2-trimethylsilylacetylene as a substrate. This substrate was employed as its steric bulk might hamper coordination of a second alkyne to the metal center, allowing us to study the first coordination event in detail.

Upon reaction of **1** with MMAO (400 eq.) and addition of 1-phenyl-2-trimethylsilylacetylene (~100 eq.), the color of the reaction mixture gradually changes from green to purple over the course of an hour (Figure S42). Interestingly, upon reaction of **1** with $AlMe_3$ (40 eq.) and addition of 1-phenyl-2-trimethylsilylacetylene (~100 eq.), no color change is observed.

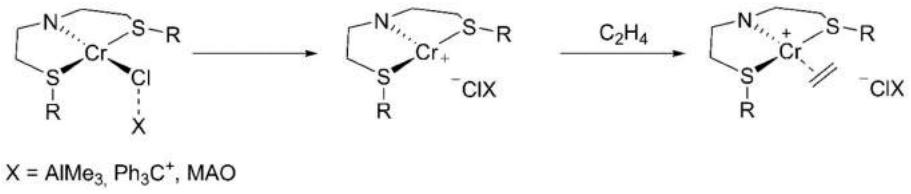

Scheme 5. Hypothesized initiation pathway, where a cationic metal center is generated via abstraction of a halide from the activated metal center.

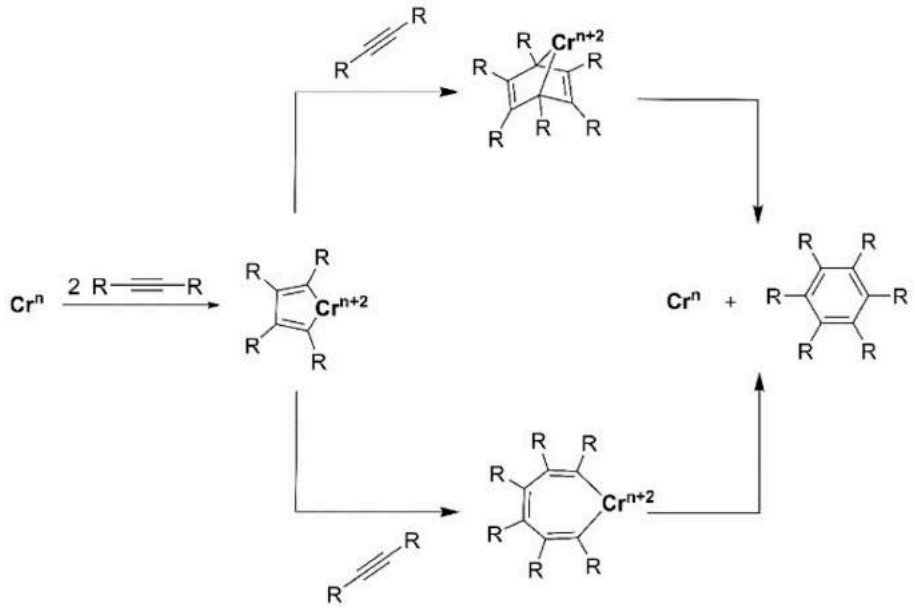

Scheme 6. Mechanism for the cyclotrimerization of alkynes. The aromatic compound is formed either via a bicyclic or a metallocycloheptatriene intermediate.

X-band EPR was applied to study the oxidation state of the metal center upon introduction of the alkyne. The experiment was performed by mixing **1** with MMAO (400 eq.) in toluene. Five minutes after activation, 1-phenyl-2-trimethylsilylacetylene (100 eq.) was added. After 2 h, an aliquot of the solution was taken and measured at 20 K. The resulting EPR spectrum is shown in Figure 2. The spectrum is composed of overlapping resonances, which can be ascribed to resonances from a Cr^{I} and a Cr^{III} complex (*vide infra*). The EPR spectrum was simulated using two components (S = 1/2 and S = 3/2). For spin counting, double integration was performed on the simulated spectra of the two components.[36] The double integral is dependent on both the effective *g*-value and different spin state as given by the relation $A_{Cr^n} \propto g_{eff}\, S(S+1)\, c_{Cr^n}$.[37–39] Here, g_{eff} represents the effective g-value, S represents the spin and c represents the concentration of the complex. For the Cr^{I} complex normalization was achieved by dividing the double integral by 1.985 (g_{eff}) and 0.75 (S = 1/2). For the Cr^{III} complex normalization was achieved by dividing the double integral by 3.317 (g_{eff}) and 3.75 (S = 3/2). The corresponding normalized double integrals were compared to the double integral of a TEMPO solution with a known concentration. The double integral determined for TEMPO was also normalized by dividing by 2.008 (g_{eff}) and 0.75 (S = 1/2). The obtained results are discussed below.

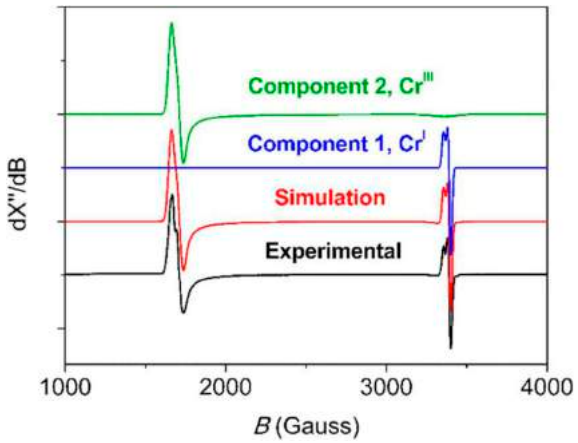

Figure 2. Experimental X-band EPR spectrum for the activation of **1** with MMAO (400 eq.), followed by the addition of 1-phenyl-2-trimethylsilylacetylene (100 eq.). The reaction was performed in toluene and was frozen after 2 hours. Also shown is the simulated spectrum and the two components used for the simulated spectrum. For the Cr^{I} complex (component 1), a fit was obtained using $g_{x,y} = 1.977$ and $g_z = 2.001$ and by applying Gaussian broadening (50 MHz). For the Cr^{III} complex (component 2), a fit was obtained using $g_x = 4.043$, $g_y = 3.914$ and $g_z = 1.995$ and by applying Gaussian broadening (221, 234 and 469 MHz respectively).

Firstly, a resonance with axial symmetry is observed ($g_{x,y} = 1.977$, $g_z = 2.002$) and was quantified to consist of ~19% of the total chromium content. The symmetry and g-values allow us to assign these resonances to the formation of bis(η^6-tolyl)Cr^{I} complexes. An additional resonance with rhombic symmetry is observed ($g_x = 4.043$, $g_y = 3.914$, $g_z = 1.995$). These resonances are expected for Cr^{III} complexes with a large zero-field splitting.[40] The concentration of this Cr^{III} complex was found to consist of ~68% of the total chromium content. A relative accuracy of ±30% is expected for quantitative EPR measurements.[11,38] Within experimental error of the measurement, it cannot be concluded whether solely these two complexes are present in solution or whether other EPR-silent complexes are also present.

Cr K-edge XAS experiments were performed to gain further insight into the structure of the formed complexes. The Cr K-edge XANES data is reported in the Supporting Information (Figure S45) and the Cr K-edge EXAFS analysis is discussed

below. The obtained parameters are presented in Table 3 and an example of the data quality is presented in Figure 3.

Care had to be taken in the EXAFS analysis, as X-band EPR spectroscopy shows the presence of (at least) a Cr^{I} complex and a Cr^{III} within the solution. We were capable of successfully fitting data by assuming that the EXAFS spectrum was composed of contributions from a five-coordinate Cr^{III} alkyne complex and a bis(η^6-tolyl)Cr^{I} complex. For the Cr^{III} alkyne complex, the best fitting results were obtained when we assumed the complex to contain 2 atoms in a Cr–C/Cr–N shell close to the metal center (~2.10 Å) and 3 atoms in a Cr–Cl/Cl–S shell (~2.40 Å). A third Cr–C shell (~3.10 Å) containing four atoms was required to fit the data. Carbon atom contained within the ligand backbone are expected to scatter at this distance from the metal center. The bis(η^6-tolyl)Cr^{I} complex is expected to contribute a Cr–C shell containing 12 atoms at a distance of 2.13 Å from the metal center.[41] This shell overlaps with the Cr–C/Cr–N shell from the Cr^{III} alkyne complex. In our fitting model we introduced a parameter (f_1) which describes the contribution (0-100%) of the bis(η^6-tolyl)Cr^{I} complex to the Cr K-edge EXAFS spectrum. Via equations given in Table 3, the coordination number of the coordination shells was related to the contribution and this parameter was optimized. The amount of bis(η^6-tolyl)Cr^{I} complex was estimated to be 8% ±11%. Within experimental error this value agrees with the value determined by EPR spectroscopy. We considered three possibilities for the structure of the reaction product. Alkynes can act as a neutral donor or can give rise to a two-electron oxidation of the metal center.[35] Either i) the alkyne directly reacts with the metal center to form a Cr^{II}/Cr^{IV} alkyne complex or ii) upon coordination of the alkyne a disproportionation reaction occurs and a Cr^{I} and a Cr^{III} complex are formed or iii) upon coordination of the alkyne a dinuclear Cr^{III} complex is formed.

The first hypothesis can be excluded due to the observation of a large quantity of Cr^{III} in the X-band EPR spectrum. The second and third hypothesis are harder to distinguish. However, if a disproportionation reaction were to occur, the amount of Cr^{III} is expected not to exceed 50%. In the performed spin counting experiments, 68% of a Cr^{III} complex is observed, deeming disproportionation unlikely. We therefore propose that the observed changes in the Cr K-edge EXAFS and X-band EPR data are due to the formation of a dinuclear Cr^{III} alkyne complex. Unfortunately, the Cr–Cr contribution of the dimer cannot be observed directly in EXAFS due to the limited EXAFS data quality and expected long Cr–Cr distance (>3.5 Å, *vide infra*).

To obtain further insights into the structure of the formed Cr^{III} alkyne complex we performed DFT–D3 calculations at the BP86/TZP level of theory for various plausible geometries (Scheme 7 and Table 4). Optimization of a neutral dinuclear Cr^{III} alkyne complex was unsuccessful. For this geometry, dissociation of one of the sulfide donors was observed. The monocationic (model I) and dicationic (model J) show very similar bond distances. They however differ in the coordination number of the Cr–Cl/Cr–S shell. Comparing the expected coordination numbers for the Cr–Cl/Cr–S shell of the monocationic (3) and dicationic (2) complex, formation of a monocationic is deemed likely based on agreement with the Cr K-edge EXAFS results.

For the monocationic Cr^{III} alkyne complex we also considered interaction of $AlMe_3$ with the chloride and amide moiety contained within the complex (Scheme 7). Formation of a dative bond between the complex and one $AlMe_3$ molecule (model K, $\Delta G = 2.9$ kcal mol^{-1}) or three $AlMe_3$ molecules (model L, $\Delta G =$

Table 3. Fitting parameters that were used to fit the obtained data for the activation of **1** with MMAO (400 eq.) in the presence of 1-phenyl-2-trimethylsilylacetylene (50 eq.).[a]

Percentage of bis(η^6-tolyl)Cr^{I} (f_1)	Coordination shell[b]	σ^2 [Å^{-2}]	d (Cr–X) [Å]
8% ± 11%	2.85 Cr–C/Cr–N[c]	0.004(3)	2.09(2)
	2.75 Cr–Cl/Cr–S[d]	0.006(1)	2.42(1)
	3.66 Cr–C[e]	0.009(4)	3.10(3)

[a] The reactions were performed at room temperature. The samples were measured as frozen solutions at a low temperature (100 K). Detailed fitting results are described in the Supporting Information (Section 4.3). [b] In these equations, f_1 is a parameter that describes the amount of bis(η^6-tolyl)Cr^{I} complex relative to a Cr^{III} alkyne complex. [c] The coordination number of the Cr–C/Cr–N shell is calculated via the equation $((12\cdot f_1)+(2\text{-}2\cdot f_1)$. [d] The coordination number of the Cr–Cl/Cr–S shell is calculated via the equation (3-3 f_1). [e] The coordination number of the Cr–C shell is calculated via the equation (4-4·f_1).

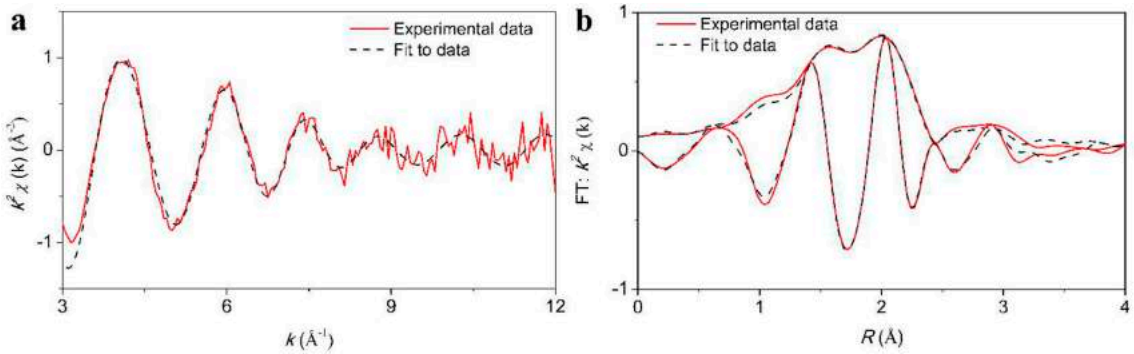

Figure 3. Cr K-edge experiments for the activation of **1** with MMAO (400 eq.), followed by the addition of 1-phenyl-2-trimethylsilylacetylene (50 eq.). The reaction was performed in toluene and was frozen after 2 hours. The reaction was performed in toluene. Depicted is a) the EXAFS data and b) the corresponding Fourier transform of k^2-weighted Cr K-edge EXAFS data. The final concentration in Cr was 3.61 mM.

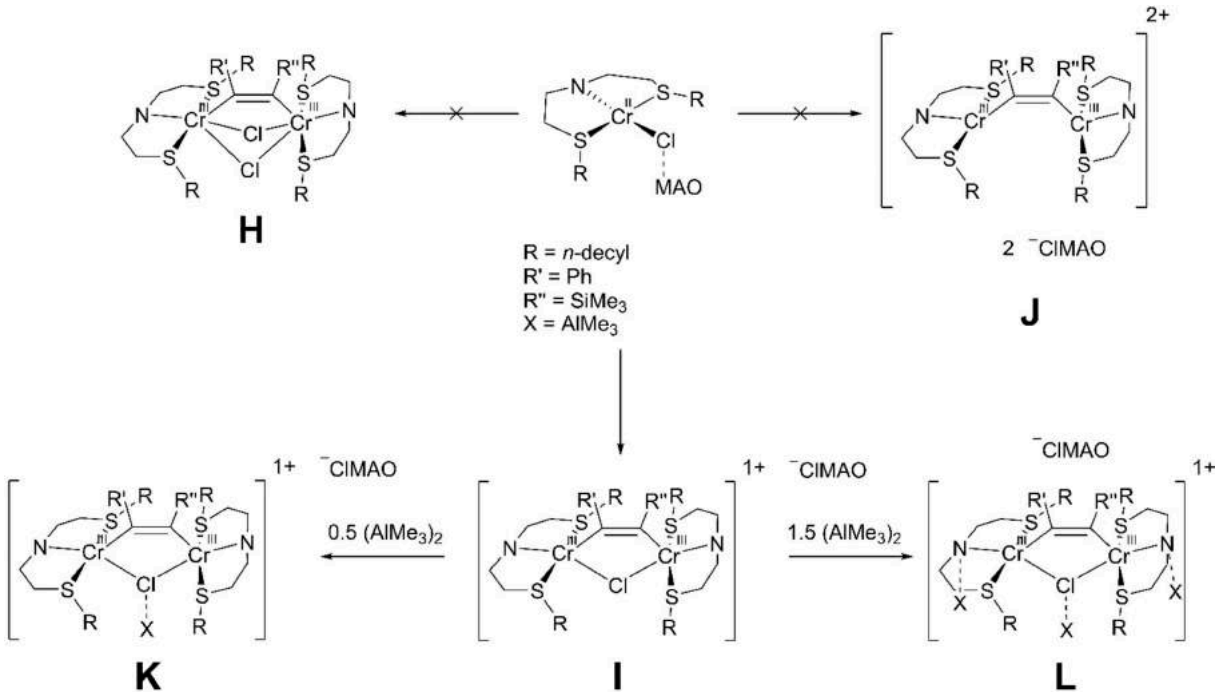

Scheme 7. Plausible reaction pathway via which the activated square-planar Cr^{II} complex can react to form a dinuclear Cr^{III} alkyne complex.

Table 4. Overview of structural parameters obtained from DFT–D3 calculations at the BP86/TZP level of theory level for various Cr^{III} complexes in the gas phase compared to the experimental Cr K-edge EXAFS data.[a]

Model	Coordination shell	*d* (Cr–X) [Å]
Experimental data	2 Cr–C/Cr–N	2.09(2)
(**1** + MMAO-12 (400 eq.) + 1-phenyl-2-trimethylsilylacetylene (50 eq.) (2 h))[b]	3 Cr–Cl/Cr–S	2.42(1)
	4 Cr–C	3.10(3)
I (monocationic)	2 Cr–C/Cr–N	1.980
	3 Cr–Cl/Cr–S	2.445
	1 Cr–Cr	3.361
J (dicationic)	2 Cr–C/Cr–N	1.985
	2 Cr–Cl/Cr–S	2.440
	1 Cr–Cr	2.674
K	2 Cr–C/Cr–N	1.987
	3 Cr–Cl/Cr–S	2.457
	1 Cr–Cr	3.510
L	2 Cr–C/Cr–N	2.062
	3 Cr–Cl	2.436
	1 Cr–Cr	3.633

[a] Geometry optimizations were performed in the absence of the anion. We considered the high-spin state in an antiferromagnetic (singlet) and ferromagnetic (heptet) configuration. The singlet and heptet spin state were found to be in close proximity to one another (~3 kcal mol^{-1}). The singlet spin state was found to be slightly more favorable and is reported in this table. [b] Given is the experimental (Cr–X) (Å) distance and the expected coordination numbers for the Cr^{III} alkyne complex, as is obtained from Cr K-edge EXAFS measurements. Samples were measured as frozen toluene solutions (100 K). Full EXAFS data analysis results are provided in the ESI.

1.2 kcal mol^{-1}) is almost neutral in energy. Close agreement between calculated and experimental Cr-C/Cr-N (experimental: 2.09(2) Å, calculated: 2.06(2) Å) and Cr–Cl/Cr–S (experimental: 2.42(1) Å, calculated: 2.457 Å) bond distance is found for model L, suggesting that this structure most closely resembles the structure of the formed Cr^{III} alkyne complex. It should be stated that the presence of bis(η^6-tolyl)Cr^{I} will give rise to a slight overestimation of the Cr–C/Cr–N bond distance.

2.4. DFT Calculations on the Mechanism of Ethene Trimerization

EPR spectroscopy and Cr K-edge XAS experiments show the oxidation of a square-planar Cr^{II} complex towards a dinuclear cationic Cr^{III} alkyne complex in the presence of 1-phenyl-2-trimethylsilylacetylene. The formation of this complex can be interpreted as being the result of dinuclear oxidative addition of the alkyne to a cationic Cr^{II} complex and a neutral Cr^{II} complex (Scheme 8). Based on these results, we were interested in whether a similar oxidation of Cr^{II} to Cr^{III} might occur in the presence of ethene. To address this question, we compared the thermochemistry of dimerization of a neutral Cr^{II} complex and a cationic Cr^{II} complex to form a dinuclear Cr^{III} complex. These DFT–D3 calculations were performed at the BP86/TZP level of theory with implicit solvent corrections (COSMO) for toluene.[42] As a bridging moiety, ethene and 1-phenyl-2-trimethylsilylacetylene were employed (Scheme 8). For 1-phenyl-2-trimethylsilylacetylene it is indeed predicted that upon coordination of 1-phenyl-2-trimethylsilylacetylene oxidation from Cr^{II} to Cr^{III} is feasible ($\Delta G = -21.8$ kcal mol^{-1}), in line with experimental observation. For ethene, an oxidation of Cr^{II} to Cr^{III} to form a dinuclear cationic Cr^{III} complex is also expected to be favored ($\Delta G = -10.8$ kcal mol^{-1}), suggesting similar reactivity could take place with ethene.

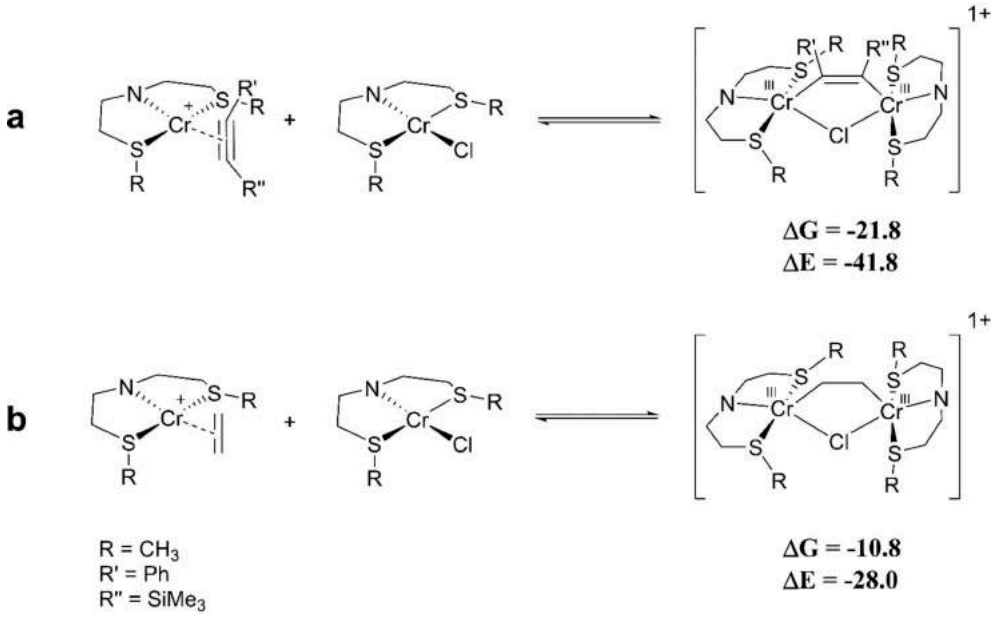

Scheme 8. DFT-D3 calculations at the BP86/TZP level of theory taking into account implicit solvent corrections (COSMO) for the oxidation of Cr^{II} to Cr^{III}. For cationic complexes, geometry optimizations were performed in the absence of an anion. For the mononuclear complexes, the high-spin state was most favored. For the dinuclear complexes we considered the high-spin state in an antiferromagnetic (singlet) and ferromagnetic (heptet) configuration. The singlet spin state is slightly favored (~3 kcal mol^{-1}). Gibbs free energies (ΔG) and electronic energies (ΔE) are reported in kcal mol^{-1}. Frequency calculations were performed at 298.15 K. Methyl substituents on the ligand were used to reduce computational cost.

These calculations raise the question of whether catalysis occurs via a cationic mononuclear Cr^{II}/Cr^{IV} redox couple or via a cationic dinuclear Cr^{II}/Cr^{III} redox couple. In recent years, mechanistic concepts for the involvement of dinuclear metallacycles in the formation of 1-octene have been brought forward by Rosenthal and coworkers.[43] The involvement of dinuclear metallacycles in ethene trimerization has also been explored by Theopold and coworkers in a Cr^{I}-{NacNac} ethene trimerization system. Two dinuclear Cr^{II} complexes containing bimetallacycles were prepared. Neither of the two complexes proved to be active for the selective trimerization of ethene. Their conclusions were that most likely ethene trimerization proceeds via a mononuclear Cr^{I}/Cr^{III} redox couple in this Cr^{I}-{NacNac} system.[44] To address the involvement of dinuclear intermediates in the {Cr(SNS)} system we resorted to DFT calculations.

It should be stated that detailed DFT calculations for the {Cr(SNS)} system have already been performed by Yang *et al.*[8] In their study they compared four plausible models: neutral Cr^{I}/Cr^{III}, monocationic Cr^{I}/Cr^{III}, monocationic Cr^{II}/Cr^{IV} and dicationic Cr^{II}/Cr^{IV} at the B3LYP/ lanl2tz/6-311G(d,p) level of theory. Of these four models, the neutral Cr^{I}/Cr^{III} model, with retention of the amine functionality, was predicted to give the lowest activation energy ($\Delta G^{\neq} = 40.1$ kcal mol^{-1}).[8,45] Based on the disagreement of their model with the experimentally observed complexes, as well as the mismatch between the calculated high activation energy found by Yang *et al.* and the observed fast reaction at 25–50 °C, we have decided to perform similar calculations for a monocationic Cr^{II}/Cr^{IV} redox couple. In addition, we have also performed calculations for a dinuclear, cationic Cr^{II}/Cr^{III} redox couple, which were not reported in the study by Yang *et al.*

The calculated mechanism for a cationic mononuclear Cr^{II}/Cr^{IV} redox couple is depicted in Figure 4. These DFT–D3 calculations were performed at the BP86/TZP level of theory. Solvent corrections were applied by performing single point calculations using an implicit solvent model for toluene (COSMO).[42] Here, we used a Cr^{II} model, with inclusion of a model for MMAO ($(AlOMe)_{10}.AlMe_3$).[30] The purpose of MMAO was to abstract the chloride from the starting complex. Calculations with other alkylaluminum compounds can be found in the Supporting Information (Section 5).

Starting from the Cr^{II} metal center **A1**, the coordination of the first (**A2**, $\Delta G = 2.8$ kcal mol^{-1}) and second ethene molecule (**A3**, $\Delta G = 20.6$ kcal mol^{-1}) to the metal are endergonic reactions, in line with experimental findings. During the coordination of the second ethene molecule, spin crossover from the quintet spin state to the triplet spin state occurs. We did not calculate the minimum energy crossing points (MECPs). In multiple publications the MECP has been demonstrated to be lower in energy than the rate-determining step.[8,46,47] Subsequent oxidative coupling of the two ethene molecules (**TSA1**, $\Delta\Delta G^{\neq} =$ 4.4 kcal mol^{-1}) yields chromacyclopentane **A4**.

Coordination of ethene to **A4** is endergonic (**A5**, ΔΔG 14.2 kcal mol^{-1}). Subsequent migratory insertion of ethene into metallacycle **A5** to yield chromacycloheptane **A6** (**TSA2**, $\Delta\Delta G^{\neq} = 7.9$ kcal mol^{-1}) is predicted to be the rate-determining step. To complete the catalytic cycle, 1-hexene is liberated via a concerted 3,7-H shift (**TSA3**, $\Delta\Delta G^{\neq} = 10.4$ kcal mol^{-1}), which is accompanied by spin crossover from the triplet to the quintet

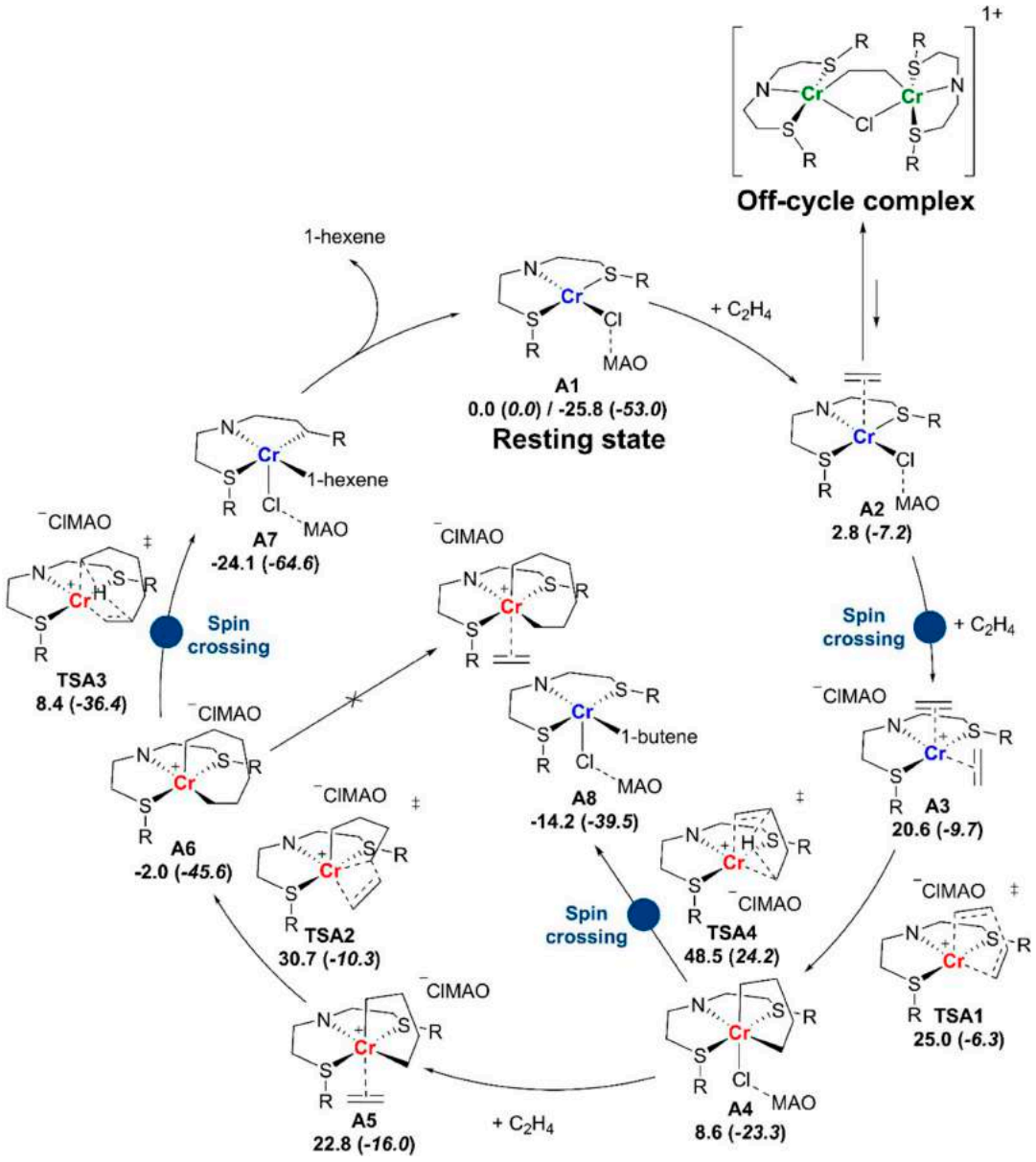

Figure 4. Model employed for DFT–D3 calculations of the mechanism for ethene trimerization via mononuclear cationic Cr^{II}/Cr^{IV} intermediates. Geometry optimization were performed at the BP86/TZP level of theory in the gas phase and solvent corrections were applied by performing single-point calculations using an implicit solvent model for toluene (COSMO). The singlet (not depicted), triplet (red) and quintet (blue) spin state were taken into account for chromium. For the dimer, the quartet (olive) spin state is depicted. Gibbs free energies and electronic energies (italics) are reported for the various intermediates of the catalytic cycle. Frequency calculations were performed at 298.15 K. Methyl substituents on the ligand were used to reduce computational cost. The model $AlOMe)_{10}.AlMe_3$ was used for MMAO, as described in reference 30.

spin state. Overall, the reaction is predicted to proceed with an activation energy of $\Delta G^{\neq} = 30.7$ kcal mol^{-1}, corresponding to the energy difference between the lowest lying intermediate **A1** and the rate-determining transition state **TSA2**.

This model is capable of correctly predicting the selectivity for 1-hexene. The formation of 1-butene from chromacyclopentane **A4** has a significantly increased barrier (**TSA4**, $\Delta\Delta G^{\neq} =$ 39.9 kcal mol^{-1}) compared to the migratory insertion of ethene to form the chromacycloheptane **A6** ($\Delta\Delta G^{\neq} = 22.1$ kcal mol^{-1}). In addition, attempts to optimize a structure with a fourth ethene molecule coordinated to chromacycloheptane **A6** failed. During geometry optimization the ethene molecule liberates from the metal center. This was also observed Yang *et al.* They ascribe this observation to the steric repulsion caused by the ligand and by the chromacyclopheptane intermediate, hampering the formation of 1-octene.[8]

An interesting finding of these calculations is that coordination of the first ethene molecule is predicted to be only mildly endergonic ($\Delta G = 2.8$ kcal mol^{-1}) at 298 K. Performing spectroscopic experiments at elevated ethene pressures and/or at lower temperatures could thus provide opportunities to stabilize these ethene-coordinated intermediates.

Some differences are observed between the calculations performed in the present study and the study performed by Yang *et al.* Firstly, the activation energy in the present study ($\Delta G^{\ddagger} = 30.7$ kcal mol^{-1}) is much lower compared to the activation energy ($\Delta G^{\ddagger} = 55.9$ kcal mol^{-1}) found by Yang *et al.* for a monocationic Cr^{II}/Cr^{IV} redox couple.[45] In addition, the activation energy found in this study also is lower compared to the neutral Cr^{I}/Cr^{III} model where the amine functionality was retained ($\Delta G^{\ddagger} = 40.1$ kcal mol^{-1}).[45] The DFT calculations performed in the present study thus provide a model in agreement with experimental findings (inclusion of activator and deprotonation of the amine functionality) and provides a physically more realistic activation energy for a reaction already proceeding at room temperature. It should however be stated that the calculated activation energy in the present study is still high for a reaction already proceeding at room temperature.

We also performed calculations for a mechanism proceeding via dinuclear cationic Cr^{II}/Cr^{III} intermediates. Our obtained results are described in detail in the Supporting Information (Section 5.5). The calculated mechanism is incapable of explaining the selectivity for 1-hexene. Very similar barriers are observed for the transition state responsible for metallacycle growth and the transition state responsible for product formation. Likely, such a dinuclear intermediate will give rise to a non-selective ethene oligo- or polymerization catalyst.

Spectroscopic studies performed in the presence of ethene have allowed for the detection of a neutral square-planar Cr^{II} complex. No ethene is coordinated to this complex. This complex likely serves as the resting state during catalysis (Figure 4). DFT calculations indicate that coordination of the first ethene molecule to this square-planar complex is endergonic. Abstraction of the bound chloride and formation of a cationic Cr^{II} complex is required to proceed through the catalytic cycle. DFT–D3 calculations show that a dinuclear ethene Cr^{III} complex could subsequently be formed under catalytic conditions (Scheme 8), which is similar in structure to the spectroscopically observed Cr^{III} alkyne complex. Calculations of a dinuclear Cr^{II}/Cr^{III} calculations however show that such a Cr^{III} ethene complex is not selective for the formation of 1-hexene and likely yields a distribution of LAOs. This dinuclear intermediate thus likely acts as an off-cycle intermediate.

Only the mechanism proceeding via mononuclear intermediates is capable of correctly predicting the observed product selectivity. Hence, this dinuclear complex most likely has to dissociate in order to generate the catalytically active mononuclear cationic Cr^{II} complex. This mononuclear Cr^{II} complex subsequently can enter the catalytic cycle (Figure 4), to produce 1-hexene in the experimentally observed selectivity.

3. Conclusions

In this study, the activation of [(R-SN(H)S–R)$CrCl_3$] with MMAO was investigated in the presence and absence of substrates (alkenes and alkynes) via the use of spectroscopic techniques (XAS, UV/VIS and EPR) and DFT calculations. In the absence of ethene, the octahedral Cr^{III} precursor is reduced to a square-planar Cr^{II} complex and the amine functionality is deprotonated. Upon introduction of ethene into the reaction mixture, no coordination of ethene is observed under the employed experimental conditions (1 bar C_2H_4). Likely this neutral Cr^{II} complex serves as the resting state during catalysis. Using an alkyne as a model for ethene coordination, oxidation from Cr^{II} to Cr^{III} is observed. This oxidation is attributed to the formation of a dinuclear cationic Cr^{III} alkyne complex. DFT calculations suggest a/similar dinuclear Cr^{III} ethene complex could form under catalytic conditions. Via DFT calculations we have compared a mechanism proceeding via cationic mononuclear Cr^{II}/Cr^{IV} intermediates to a mechanism proceeding via cationic dinuclear Cr^{II}/Cr^{III} intermediates. Only the mononuclear Cr^{II}/Cr^{IV} mechanism is capable of correctly predicting the observed product selectivity. Future studies will focus on stabilizing the proposed cationic Cr ethene complexes. We aim to achieve this by performing the activation in the presence of ethene at elevated ethene pressures and/or lower temperatures.

Experimental Section

The experimental details are reported in the Supporting Information.

Acknowledgements

The authors thank NWO for funding (VIDI grant 723.014.010 (to M.T., B.V., J.P.O., D.J.M.) and VENI grant 722.016.012 (to T.J.K.). The authors thank the staff of the beamlines SuperXAS, Swiss Light Source (proposal number 20160674) in Villigen, Switzerland and B18, Diamond Light Source (proposal number SP15305) in Didcot, UK for support and access to their facilities. The authors thank Michelle Hammerton and Lukas Wolzak for support during synchrotron measurements. The authors thank Jan-Meine Ernsting, Andreas Ehlers and Ed Zuidinga for NMR spectroscopy and mass spectrometry support. The authors thank Andreas Ehlers for support with the performed DFT calculations.

Conflict of Interest

The authors declare no conflict of interest.

Keywords: EPR spectroscopy · XAS spectroscopy · trimerization · chromium · reaction mechanisms

[1] *Grand View Research, Alpha Olefin Market Analysis By Product, (1-Butene, 1-Hexene, 1-Octene, 1-Decene, 1-Dodecene), By Application (Polyethylene, Detergent Alcohol, Synthetic Lubricants), By Region, And Segment Forecasts*, 2018–2025, **2017**.
[2] D. S. McGuinness, *Chem. Rev.* **2011**, *111*, 2321–2341.
[3] T. Agapie, *Coord. Chem. Rev.* **2011**, *255*, 861–880.
[4] O. L. Sydora, *Organometallics* **2019**, *38*, 997–1010.
[5] K. A. Alferov, G. P. Belov, Y. Meng, *Appl. Catal. A* **2017**, *542*, 71–124.
[6] J. R. Briggs, *J. Chem. Soc. Chem. Commun.* **1989**, *0*, 674.

[7] T. Agapie, J. A. Labinger, J. E. Bercaw, *J. Am. Chem. Soc.* **2007**, *129*, 14281–14295.
[8] Y. Yang, Z. Liu, L. Zhong, P. Qiu, Q. Dong, R. Cheng, J. Vanderbilt, B. Liu, *Organometallics* **2011**, *30*, 5297–5302.
[9] A. Jabri, C. B. Mason, Y. Sim, S. Gambarotta, T. J. Burchell, R. Duchateau, *Angew. Chem. Int. Ed.* **2008**, *47*, 9717–9721; *Angew. Chem.* **2008**, *120*, 9863–9867.
[10] K. Albahily, Y. Shaikh, Z. Ahmed, I. Korobkov, S. Gambarotta, R. Duchateau, *Organometallics* **2011**, *30*, 4159–4164.
[11] I. Y. Skobelev, V. N. Panchenko, O. Y. Lyakin, K. P. Bryliakov, V. A. Zakharov, E. P. Talsi, *Organometallics* **2010**, *29*, 2943–2950.
[12] J. Rabeah, M. Bauer, W. Baumann, A. E. C. McConnell, W. F. Gabrielli, P. B. Webb, D. Selent, A. Brückner, *ACS Catal.* **2013**, *3*, 95–102.
[13] W. J. Van Rensburg, C. Grové, J. P. Steynberg, K. B. Stark, J. J. Huyser, P. J. Steynberg, *Organometallics* **2004**, *23*, 1207–1222.
[14] A. Brückner, J. K. Jabor, A. E. C. McConnell, P. B. Webb, *Organometallics* **2008**, *27*, 3849–3856.
[15] J. Telser, L. A. Pardi, J. Krzystek, L.-C. Brunel, *Inorg. Chem.* **2000**, *39*, 1834–1834.
[16] S. N. MacMillan, K. M. Lancaster, *ACS Catal.* **2017**, 7, 1776–1791.
[17] M. Tromp, J. Moulin, G. Reid, J. Evans, *AIP Conf. Proc.,* **2007**, pp. 699–701.
[18] S. A. Bartlett, P. P. Wells, M. Nachtegaal, A. J. Dent, G. Cibin, G. Reid, J. Evans, M. Tromp, *J. Catal.* **2011**, *284*, 247–258.
[19] S. A. Bartlett, J. Moulin, M. Tromp, G. Reid, A. J. Dent, G. Cibin, D. S. McGuinness, J. Evans, *Catal. Sci. Technol.* **2016**, *6*, 6237–6246.
[20] B. Venderbosch, J. P. H. Oudsen, L. A. Wolzak, D. J. Martin, T. J. Korstanje, M. Tromp, *ACS Catal.* **2019**, *9*, 1197–1210.
[21] S. A. Bartlett, J. Moulin, M. Tromp, G. Reid, A. J. Dent, G. Cibin, D. S. McGuinness, J. Evans, *ACS Catal.* **2014**, *4*, 4201–4204.
[22] D. S. McGuinness, P. Wasserscheid, W. Keim, D. Morgan, J. T. Dixon, A. Bollmann, H. Maumela, F. Hess, U. Englert, *J. Am. Chem. Soc.* **2003**, *125*, 5272–5273.
[23] D. S. McGuinness, D. B. Brown, R. P. Tooze, F. M. Hess, J. T. Dixon, A. M. Z. Slawin, *Organometallics* **2006**, *25*, 3605–3610.
[24] I. Krossing, H. Brands, R. Feuerhake, S. Koenig, *J. Fluorine Chem.* **2001**, *112*, 83–90.
[25] D. S. McGuinness, A. J. Rucklidge, R. P. Tooze, A. M. Z. Slawin, *Organometallics* **2007**, *26*, 2561–2569.
[26] H. Hagen, W. P. Kretschmer, F. R. van Buren, B. Hessen, D. A. van Oeffelen, *J. Mol. Catal. A* **2006**, *248*, 237–247.
[27] N. B. Bespalova, D. N. Cheredilin, A. M. Sheloumov, G. A. Kozlova, A. A. Senin, I. I. Khasbiullin, *Catalyst System for Trimerisation of Ethylene into 1-Hexene Using Catalysts with Branched Hydrocarbon Skeleton*, **2015**, RU2556640C1.
[28] A. R. Barron, *Organometallics* **1995**, *14*, 3581–3583.
[29] W. J. Van Rensburg, J. A. Van Den Berg, P. J. Steynberg, *Organometallics* **2007**, *26*, 1000–1013.
[30] Z. Falls, N. Tymińska, E. Zurek, *Macromolecules* **2014**, *47*, 8556–8569.
[31] T. Gunasekara, J. Kim, A. Preston, D. K. Steelman, G. A. Medvedev, W. N. Delgass, O. L. Sydora, J. M. Caruthers, M. M. Abu-Omar, *ACS Catal.* **2018**, *8*, 6810–6819.
[32] L. H. Do, J. A. Labinger, J. E. Bercaw, *ACS Catal.* **2013**, *3*, 2582–2585.
[33] R. M. Fuoss, *J. Am. Chem. Soc.* **1958**, *80*, 5059–5061.
[34] D. L. J. Broere, E. Ruijter, *Synth.* **2012**, *44*, 2639–2672.
[35] K. Yamamoto, H. Nagae, H. Tsurugi, K. Mashima, *Dalton Trans.* **2016**, *45*, 17072–17081.
[36] M. R. Gafurov, I. N. Mukhambetov, B. V. Yavkin, G. V. Mamin, A. A. Lamberov, S. B. Orlinskii, *J. Phys. Chem. C* **2015**, *119*, 27410–27415.
[37] R. Aasa, T. Vänngård, *J. Magn. Reson.* **1975**, *19*, 308–315.
[38] G. Sabenya, L. Lázaro, I. Gamba, V. Martin-Diaconescu, E. Andris, T. Weyhermüller, F. Neese, J. Roithova, E. Bill, J. Lloret-Fillol, *J. Am. Chem. Soc.* **2017**, *139*, 9168–9177.
[39] E. Morra, G. A. Martino, A. Piovano, C. Barzan, E. Groppo, M. Chiesa, *J. Phys. Chem. C* **2018**, *122*, 21531–21536.
[40] N. Shaham, H. Cohen, D. Meyerstein, E. Bill, *J. Chem. Soc. Dalton Trans.* **2000**, *0*, 3082–3085.
[41] B. Morosin, *Acta Crystallogr. Sect. B Struct. Crystallogr. Cryst. Chem.* **1974**, *30*, 838–839.
[42] V. Barone, M. Cossi, *J. Phys. Chem. A* **1998**, *102*, 1995–2001.
[43] S. Peitz, B. R. Aluri, N. Peulecke, B. H. Müller, A. Wöhl, W. Müller, M. H. Al-Hazmi, F. M. Mosa, U. Rosenthal, *Chem.-A Eur. J.* **2010**, *16*, 7670–7676.
[44] W. H. Monillas, J. F. Young, G. P. A. Yap, K. H. Theopold, *Dalton Trans.* **2013**, *42*, 9198–9210.
[45] The activation energy was evaluated by calculating the difference in Gibbs free energy between the intermediate lowest in energy and the transition state highest in energy on the lowest lying spin surface. These values were supplied in the Supporting Information of reference 8. A similar definition for the activation energy is employed in the present study.
[46] M. Gong, Z. Liu, Y. Li, Y. Ma, Q. Sun, J. Zhang, B. Liu, *Organometallics* **2016**, *35*, 972–981.
[47] G. J. P. Britovsek, D. S. McGuinness, T. S. Wierenga, C. T. Young, *ACS Catal.* **2015**, *5*, 4152–4166.

Manuscript received: August 30, 2019
Revised manuscript received: October 16, 2019
Accepted manuscript online: October 16, 2019
Version of record online: December 12, 2019